Journal of Wind Engineering & Industrial Aerodynamics 228 (2022) 105113

Contents lists available at ScienceDirect

Journal of Wind Engineering & Industrial Aerodynamics

journal homepage: www.elsevier.com/locate/jweia

Thrust-matched optimization of blades for the reduced-scale wind tunnel tests of wind turbine wakes

Guoqing Huang [a], Senqin Zhang [a,c], Bowen Yan [a,*], Qingshan Yang [a], Xuhong Zhou [a], Takeshi Ishihara [b]

[a] Chongqing Key Laboratory of Wind Engineering and Wind Energy Utilization, School of Civil Engineering, Chongqing University, Chongqing, 400045, China
[b] Department of Civil Engineering, School of Engineering, The University of Tokyo, 7-3-1, Hongo, Bunkyo-ku, Tokyo, Japan
[c] Energy Research Institute, Qilu University of Technology (Shandong Academy of Sciences), Jinan, Shandong, 250014, China

ARTICLE INFO

Keywords:
Wind turbine wake
Thrust coefficient
Wind tunnel experiment
Blade
Optimization

ABSTRACT

This study proposes a thrust-matched optimization methodology of wind turbine blades to accurately reproduce the wind turbine wake characteristics in the reduced-scale wind tunnel experiment. The scaled models with scale ratio of 1:250 for two wind turbines (5 MW and 2 MW) from the industrial community are produced by the proposed optimization methodology for validation purposes. In addition, the wake characteristics of the scaled wind turbine model are experimentally measured and discussed against the analytical wake model. The results show that the wake from the experiment is consistent with that predicted by the wake model, verifying the rationality and feasibility of the proposed optimization method. Also, the effects of upstream turbulence on the wind turbine wakes and the declining wake center in the vertical direction could be satisfactorily reproduced and revealed in the wind tunnel tests.

1. Introduction

In the large-scale wind farm consisting of dozens of closely-arranged wind turbines, wake effects could significantly reduce the power production (Lyu et al., 2019; Xiong et al., 2020). Meanwhile, the increased turbulence intensity in the turbine wake would shorten the service life of the wind turbine due to the increased structural fatigue (Hui et al., 2012; Iungo, 2016). Therefore, it has attracted increasing attention to numerically and experimentally investigate the wind turbine wake in past decades (Jensen, 1983; Crespo et al., 1999; Medici and Alfredsson., 2006; Dobrev et al., 2008; Chamorro and Porte-Agel, 2009; Shamsoddin and Porté-Agel, 2020).

The thrust coefficient is of utmost importance among many parameters affecting the wake characteristics of a wind turbine. Ishihara and Qian (2018) conducted full-scale numerical simulations of the 2 MW wind turbine wake characteristics and have verified that the small-scale wind turbine model that satisfied the consistent thrust force coefficient with the corresponding full-scale one could reproduce the reasonable wake characteristics. In the wind tunnel experiment of wind turbine wake, the thrust coefficients of geometrically-scaled blades could hardly meet the prescribed prototype value, particularly at a small-scale ratio (Martin, 2011; Duan et al., 2016; Ishihara and Qian, 2018). As a result, it is challenging to make thrust coefficients of the reduced-scale blades in the wind tunnel tests coincide with those of the full-scale ones.

In the previous studies of wind turbine wakes, the porous disc was designed to match the constant thrust coefficient of an operating wind turbine (Howland et al., 2016). However, it failed to consider the rotational effect of the wind turbine blades (Xie and Archer, 2015). Ishihara et al. (2004) chose the low Reynolds-number blade and adjusted the pitch angle of the blades to match the thrust coefficient of the prototype 2 MW wind turbine. However, whether the effect of changing pitch angle on improving the thrust coefficient of the scaled wind turbine model is suitable for the scaled model of the large-scale wind turbine in the wind tunnel tests is worth further study.

Apart from the wind turbine wake experiment, the design of the thrust-matched blade is also important for the dynamic response experiment of the scaled floating wind turbine where the Froude similarity is maintained in the coupled wind/wave environment (Martin, 2011; 2014; Li et al., 2021). They proposed an optimization methodology for scaled wind turbine blades in the Froude-scale test. The flat and low Reynolds Number airfoil was redesigned for the Froude-scale model by coupling aerodynamic force coefficients analysis and the genetic algorithm (GA)-based optimization. The validation results showed that

* Corresponding author.
E-mail addresses: ghuang1001@gmail.com (G. Huang), bowenyancq@cqu.edu.cn (B. Yan).

https://doi.org/10.1016/j.jweia.2022.105113
Received 6 January 2022; Received in revised form 24 July 2022; Accepted 24 July 2022

Nomenclature

I_u	Turbulence intensities
D	Rotor diameter
T	The thrust force of wind turbine
U_{hub}	The wind speed at the hub height
$(-)_p$	The quantity corresponding to prototype one
$X(-)$	Optimization parameters
z_{hub}	Hub height
T_{rb}	The thrust force under the rotating state
T_{rn}	The thrust force of nacelle and tower (without blades)
T_{nb}	The thrust force of the operating wind turbine without incoming wind
R	The radius of the wind turbine rotor
β	Pitch angle
C_L	The lift force coefficient
C_D	The drag force coefficient
$c(r)$	The chord length of the blade
$\theta(r)$	The twist angle
ω	The rotor angular speed
C_T	The thrust force coefficient
ABL	Atmospheric Boundary Layer
NGW	New Gaussian wake model
ALM	Actuator line model
CTA	Constant temperature hot wire anemometer
AOA	Angle of attack
TSR	The tip-speed ratio

the optimization method produced the scaled wind turbine blades with a similar thrust coefficient to the full-scale ones. Due to the good performance, this method is adapted to the wind tunnel test of wind turbine wakes in this study.

It is noted that a large scale-ratio of 1:50 was used in the aforementioned experiment on the floating wind turbine. In contrast, a smaller scale ratio of 1:200–1:400 is usually adopted in wind turbine wake experiments (Yang et al., 2011; Tian et al., 2018). When the tip-speed ratio in the small-scale model is the same as that in the full-scale wind turbine, the rotor speed is as fast as the order of 10^3 rpm, resulting in a high angle of attack (AOA) for blade airfoils. Under such a scenario, strong separation bubbles and significantly unsteady turbulence would occur around the airfoil (Shi et al., 2021). It poses a great challenge to accurately predict the aerodynamic performance of the airfoil since the aerodynamic performance analysis in the previous work (Martin et al., 2014) was mainly intended for the laminar boundary layer flow with the limit range of AOA (-5° to 10°). As a result, the applicability of the blade optimization methodology for Froude scale tests remains unclear in the wind tunnel tests of turbine wakes with a small scale ratio.

This study aims to put forward a blade optimization methodology suited to the small-scale wind tunnel test of turbine wakes. In this methodology, the Viterna method (Viterna and Janetzke, 1982) is adopted to numerically extrapolate the aerodynamic force coefficients from the limited range of AOA of blades to the extended AOA range; then the multi-objective pattern search algorithm is embedded with the blade-element theory (BEM) code for the thrust force coefficients of the small-scale blade with the rapid rotor speed. Based on this proposed methodology, the redesign of two types of wind turbines (D151-5 MW wind turbine with a rotor diameter of 151m and D120-2 MW wind turbine with a rotor diameter of 120m) in model scale is conducted. Furthermore, the thrust coefficients of geometrically-scale and thrust-matched blades are measured in the wind tunnel tests for validation and comparison purposes. Moreover, the spatial distributions of wake deficit velocity and turbulence intensity of the D151-5 MW turbine model under different upstream flow conditions are experimentally verified against the analytical wake model.

2. Optimization methodology

This section introduces the optimization methodology of blades for the wind tunnel experiment in the wake of the small-scale wind turbine model.

The proposed optimization methodology aims to produce the blades of a scaled wind turbine model (the scale ratio of 1: m) with the thrust coefficient C_T satisfying the design blade tip-speed ratio (TSR). In this study, the design TSR is the same as the prototype TSR. C_T and TSR for the scaled blade are defined as follows:

$$C_T = \frac{T}{0.5\rho U_{hub}{}^2 A} \tag{1}$$

$$TSR = \frac{\omega R}{U_{hub}} \tag{2}$$

where T is the thrust forces on the wind turbine blades, ρ is the air density, A is the swept area of the rotor, U_{hub} is the mean wind speed at the hub height, ω is the rotor angular speed and R is the radius of the wind turbine rotor. With corresponding parameters, C_T and TSR for the prototype blade can be obtained.

The main variables affecting the thrust coefficient C_T are the blade length, rotor speed, pitch angle, airfoil type, chord length, and twist angle of the blade. In this study, the blade length would be geometrically scaled to meet the requirement of geometric similarity. The rotor speed would then be determined according to the kinematic similarity with the same TSR as the prototype one. The pitch angle is the same as the prototype blades. In the following optimization framework, the proper airfoil type is firstly selected from the airfoil database with the reference to the full-scale one, then the chord length and twist angle are chosen as variables in the optimization algorithm to match the prototype values of C_T.

Regarding the airfoil type, the flat one would first be chosen to ensure the higher aerodynamic force coefficients of C_L (lift coefficient) and C_D (drag coefficient) at a low Reynolds number (nominally, Re in the range of 10^4). The Viterna method is used to extrapolate the aerodynamic force coefficient obtained from the Xfoil for AOA of -10^o to 20^o, to the extended AOA range of -180^o to 180^o (Drela, 1989). The equations of C_D and C_L by the Viterna method are summarized as follows:

$$B_2 = \frac{C_{Ds} - C_{D\max}\sin^2\alpha_s}{\cos\alpha_s} \tag{3}$$

$$C_{D\max} = 1.11 + 0.018AR \tag{4}$$

$$C_D = C_{D\max}\sin^2\alpha + B_2\cos\alpha \tag{5}$$

$$A_2 = (C_{Ds} - C_{D\max}\sin\alpha_s\cos\alpha_s)\frac{\sin\alpha_s}{\cos^2\alpha_s} \tag{6}$$

$$C_L = \frac{C_{D\max}}{2}\sin 2\alpha + A_2\frac{\cos^2\alpha}{\sin\alpha} \tag{7}$$

where C_{Dmax} is the maximum resistance coefficient, α is the angle of attack, B_2 is the correction coefficient; subscript s stands for stall point or matching point; AR is the aspect ratio.

In the flow chart of the optimization framework as shown in Fig. 1, the chord length $c(r)$ and twist angle $\theta(r)$ are chosen as variables where r

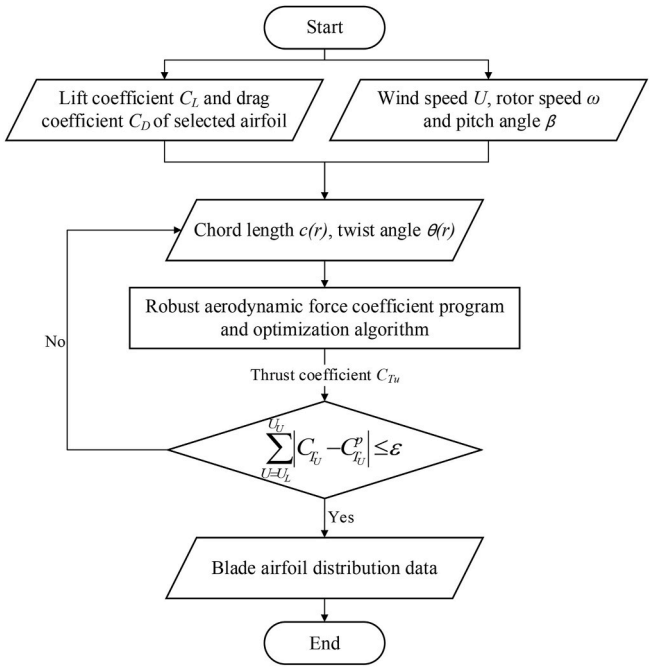

Fig. 1. Flow chart of the optimization framework.

is the radial coordinate of the scaled blade. The optimal solution to minimize the difference between thrust coefficients of scaled and prototype blades can be found by the multi-objective pattern search algorithm under the limiting conditions, which is shown in Eqs. 8–10. In the optimization procedure, the in-house code specifically for a small-scale blade with a rapid rotor speed is also developed based on the BEM theory to avoid the numerical divergence of the general-purpose aerodynamic performance analysis tool adopted in the previous work (Jonkman et al., 2005). The chord length varies along the prototype blade and can be described by the distribution function $c^p(mr)$ in Eq. (8). An unknown variable $X(1)$ in the distribution function $c(r)$ is iteratively determined in the optimization algorithm by proportionally scaling the chord length of the geometrically-scaled prototype blade. Via this treatment, a similar chord length could be maintained between the scaled blade and the prototype one. For the twisted angle, the distribution curve $\theta(r)$ of the prototype blade approximately follows the quadratic polynomial function (Fowler et al., 2013) as shown in Eq. (8). Hence, the unknown vairbales of $X(2)$, $X(3)$, and $X(4)$ in the distribution curve of the twist angle $\theta(r)$ can be nonlinearly regressed with the quadratic polynomial function.

$$\begin{aligned} &\text{Find} \quad c(r) = X(1)c^p(mr)/m, \quad 0 \le r \le R \\ &\quad\;\; \theta(r) = X(2)r^2 + X(3)r + X(4), \quad 0 \le r \le R \end{aligned} \tag{8}$$

$$\text{Minimize } f(\theta, c) = \int_{U_L}^{U_U} |C_T(U) - C_T^p(U)| dU \tag{9}$$

$$\begin{aligned} &\text{Constraints} \quad \theta_L(r) \le \theta(r) \le \theta_U(r) \\ &\quad\;\; \lim_{r \to R} \theta(r) = 0 \end{aligned} \tag{10}$$

where R is the scaled blade radius, U is the incoming wind speed, U_L and U_U are the lower and upper bounds for the operating range of incoming wind speed, respectively. $C_T(U)$ and $C_T^p(U)$ are the thrust coefficient of the model-scaled and full-scale wind turbine, respectively. $\theta_L(r)$ and $\theta_U(r)$ are the lower and upper bounds of the twist angle distribution, respectively.

3. Model blade design examples

In this section, two types of blades for offshore wind turbines (D151-5 MW and D120-2 MW) from practical engineering are redesigned using the proposed optimization methodology for validation purposes. The scale ratio of the model blade is 1:250, which is determined by satisfying the requirement of blockage ratio and preventing the wall constraint effects for turbine wake evolutions. The wind speed ratio is 1:1. For the prototype turbine, the cut-in wind speed is 4 m/s and the thrust coefficient above 12 m/s is relatively small. Hence, the thrust coefficients within the range of 4–12 m/s are adopted in the optimization procedure. Note that TSR is 12.1 and 7.5 for 4 m/s and 12 m/s, respectively.

The first step is to choose the appropriate airfoil type for scaled blades. The prototype blade has 10 airfoil types in which the reference airfoil accounts for 44% of the whole blade length as shown in Fig. 2(a). The reference airfoil as depicted in Fig. 3 is adopted in the selection of low Reynolds number airfoil in the subsequent section. Fig. 2(b) shows the thrust-matched blade. Fig. 3(a) shows airfoils of prototype blade and thrust-matched blade for 5 MW turbine. Fig. 3(b)–(d) illustrates the prototype blade of a 5 MW wind turbine, the redesigned and thrust-matched blade of a 5 MW wind turbine, and the redesigned and thrust-matched blade of a 2 MW wind turbine, respectively.

Under the rated wind speed of 10.4 m/s, the Reynolds number (Re) based on the average chord length and the incoming wind speed at the hub height (U_{hub}) for the prototype blade is estimated to be 5.0×10^6; meanwhile, the corresponding Re is 2.0×10^4 for the model test in this study. Fig. 4 shows the comparison of aerodynamic force coefficients of reference airfoil between the full-scale and model-scale. The value of C_D is not sensitive to the large variation of the Reynolds number (Re) as demonstrated in Fig. 4(a). On the contrary, Fig. 4(b) shows the C_L of the prototype airfoil is almost 2.5 times larger than that of the geometrically-scaled airfoil. This difference in aerodynamic force coefficients between the prototype and scaled airfoil is also confirmed by the previous study by Martin (2011). Therefore, it is of utmost importance to choose the low Reynolds number airfoil, which has similar lift and drag coefficients to the prototype one. In this study, the low Reynolds number airfoil of NACA6409 is chosen from the NACA airfoil library (http://www.airfoiltools.com), whose aerodynamic force coefficients at the model scale are close to those of the prototype reference airfoil.

Secondly, in the optimization of the scaled blade, the chord length and twist angle are used to adjust the selected NACA6409 airfoil along the blade. Theoretically, there are multiple combinations of the chord length and twist angle to meet the target thrust coefficient. However, most of them have the discontinuous chord length and twist angles along the blade, which makes blade production impossible. In the design of the practical model blade, the continuous distribution for both chord length and twist angle can be obtained following the requirement in Section 2. Hence, a total of four unknowns in Eq. (8) should be iteratively regressed via the optimization procedure.

Thirdly, the pattern search method combined with the self-developed numerical program for aerodynamic force coefficients of small-scale blades is used to determine the optimal solutions of chord length and twist angle. After optimization, the aerodynamic performance of the blade agrees well with the expected results, and the distributions of blade chord and twist angle are smooth and continuous. The optimization framework proposed in this study is cost-effective, which could be accomplished within 60–100 iterations for the optimization process. Both the distributions of the blade chord and twist angle of thrust-matched and prototype blades are shown in Fig. 5.

The numerical validations of thrust coefficients between the scaled and prototype blades for the D151-5 MW wind turbine are shown in Fig. 6. Besides, the scaled blades of the D120-2 MW wind turbine are also redesigned by the proposed optimization methodology to verify its generality. The comparison of thrust coefficients between the scaled and prototype blades for D120-2 MW is also shown in Fig. 6. The results

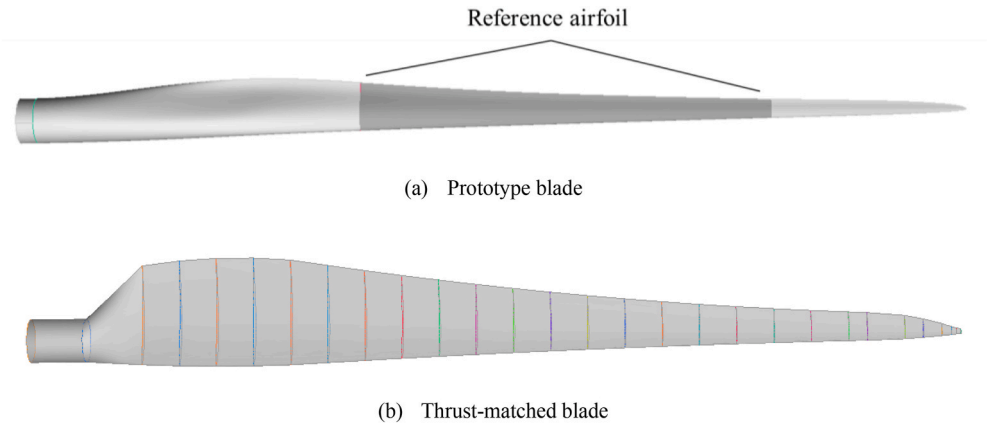

Fig. 2. 3D models of geometrically scaled prototype blade and thrust-matched blade.

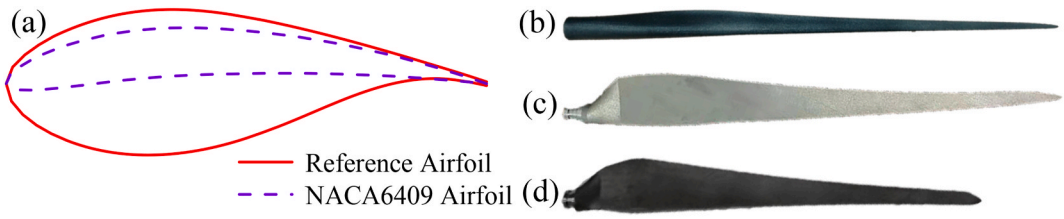

Fig. 3. Airfoils and blades of turbines: a. The airfoil of reference blade and thrust-matched blade for 5 MW turbine; b. Prototype blade of 5 MW wind turbine; c. Redesigned and thrust-matched blade of 5 MW wind turbine; d. Redesigned and thrust-matched blade of 2 MW wind turbine.

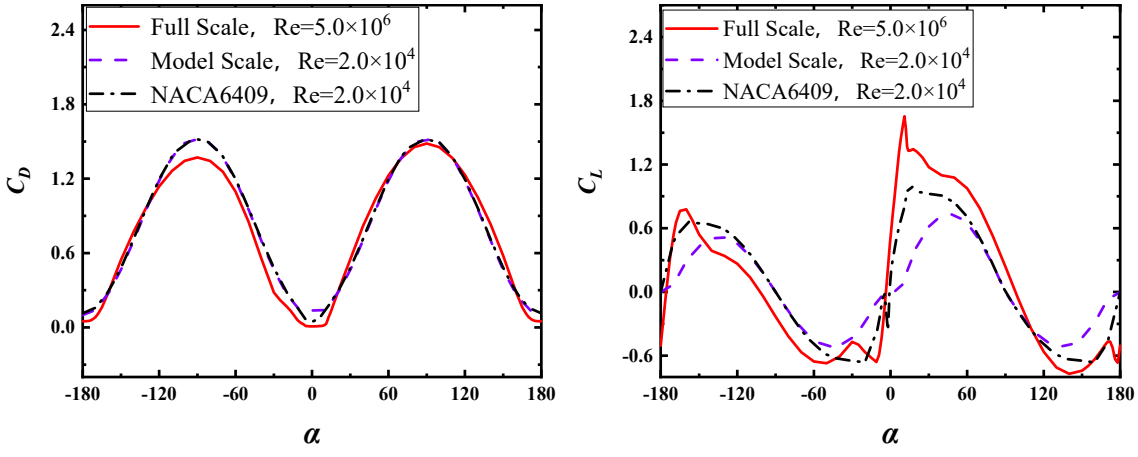

Fig. 4. Drag and lift coefficients of reference airfoil in full-scale, model scale, and NACA6409 airfoils.

show that the thrust coefficients of the scaled blades of both D151-5 MW and D120-2 MW wind turbines agree well with those of the prototype ones, indicating that the proposed optimization methodology has excellent performance.

4. Experimental set-up of wind tunnel tests

The experiment for the scaled wind turbine model is conducted in the wind tunnel of Chongqing University (CQU), which is illustrated in Fig. 7. The dimensions of the wind tunnel test section are 2.4 m (wide) × 1.8 m (high) × 15.1 m (long), and the maximum wind speed of the wind tunnel is 45 m/s. The blockage ratio of the wind turbine model to the wind tunnel cross-sectional area is about 6.5%, indicating that the confinement effect of the wind tunnel walls on the turbine wake is negligible (Bastankhah and Porté-Agel, 2016).

Various large-scale mesh grids at the inlet of the wind tunnel test section are used to generate atmospheric boundary-layer (ABL) flows, as illustrated in Fig. 7. Fig. 8(a) shows two types of emulated ABL flows following the power law of $U_z/U_{hub} = (z/z_{hub})^{\alpha}$ where U_z and U_{hub} are the incoming wind speed at height z and hub height z_{hub}. Meanwhile, the corresponding turbulence intensities $I_{u,hub}$ at the hub height are 2% and 6%, respectively. Fig. 8(c) shows the power spectrum of the incoming fluctuating velocity measured at turbine hub height, which agrees well with Karman spectral model. The roughness length (z_0) is 9.33×10^{-5} m and the friction velocity (u^*) is 0.45 m/s. Fig. 8 (d) shows the Reynolds normal and shear stresses.

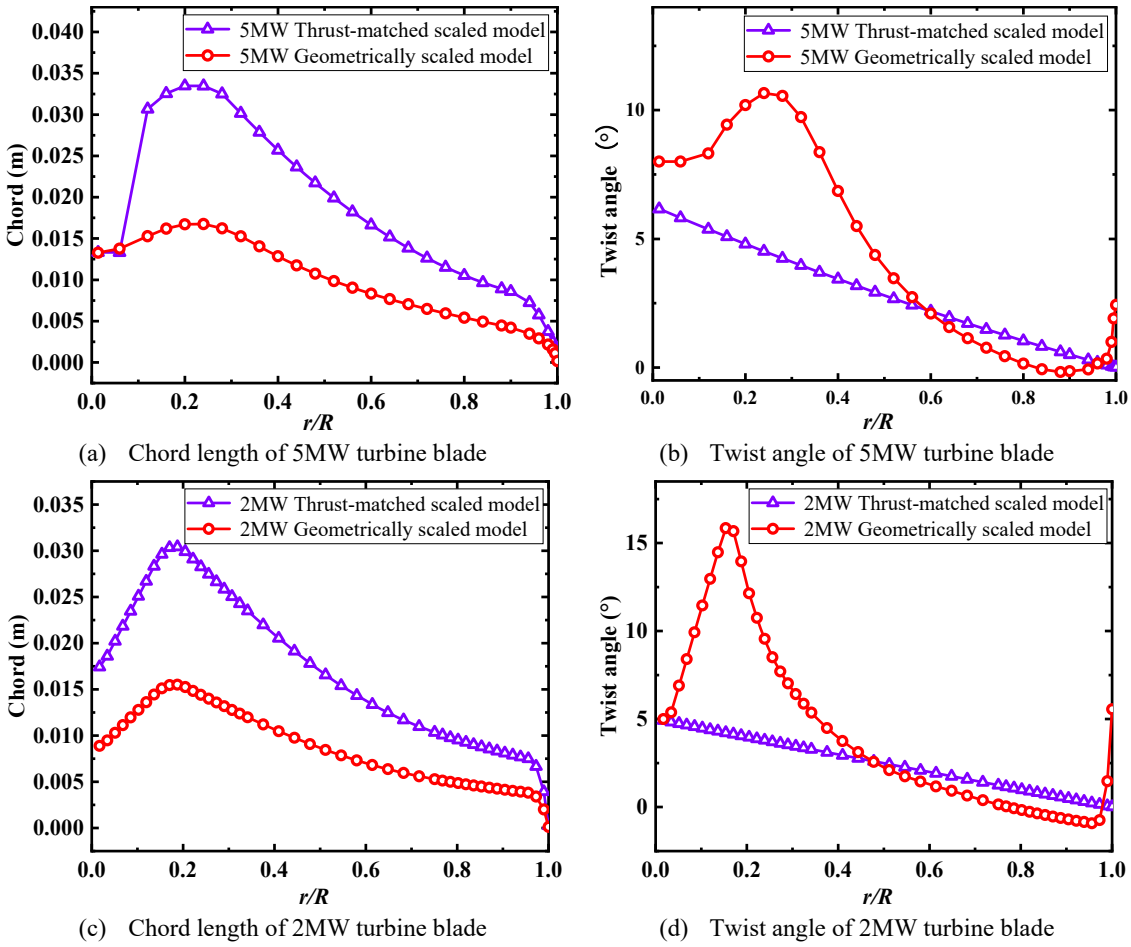

Fig. 5. Distributions of blade chord and twist angle.

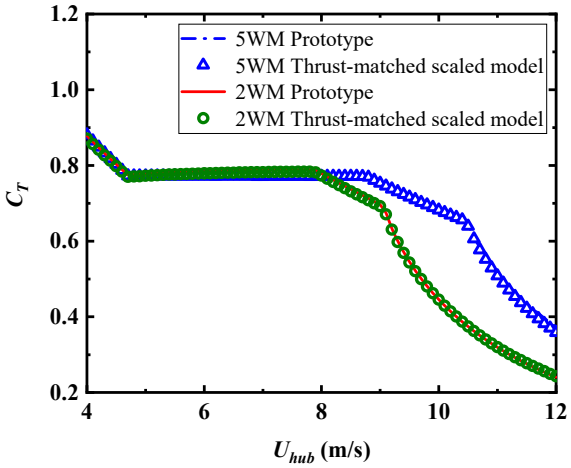

Fig. 6. Thrust coefficient of thrust-matched blades.

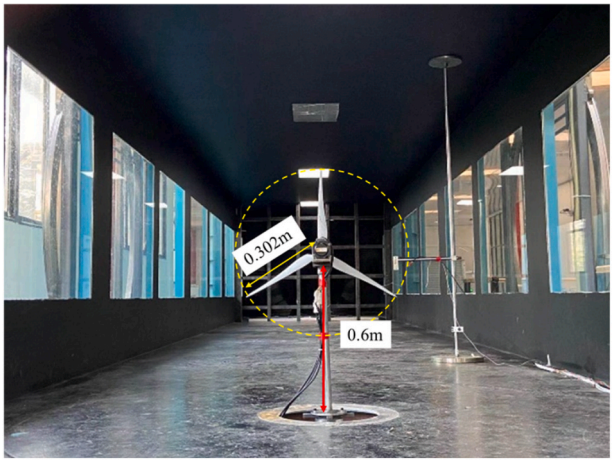

Fig. 7. Photograph of scale wind turbine model in wind tunnel of CQU.

The rotor diameter D and the hub height z_{hub} are 0.604 m and 0.6 m, respectively as shown in Fig. 7, and it is quite common to adopt the hub height and rotor diameter as the reference characteristic length in the study of wind turbine wakes (Lanzilao and Meyers, 2022). The fabrication of the wind turbine model is as follows: (1) the support tower, base plate, and nacelle are made of steel for its monolithic safety; (2) the advanced 3D printing technology is adopted to accurately mimic the thrust-matched blades to achieve the structural integrity and stiffness during the tests. The three-blade model wind turbine is placed 9 m downwind of the entrance of the test section. The turbine rotor is driven by an AC Servo motor to generate the corresponding rotor speed. For this motor, the rated and maximum rotation speeds are 3000 rpm and 6000 rpm, respectively, and the maximum torque is 1.11 Nm. In the test, the *TSR* is the same as that of the prototype wind turbine to ensure the kinematic similarity. Accordingly, the maximum rotor speed of the wind turbine reaches as high as 2835 rpm when U_{hub} is larger than the rated wind speed of 10.4 m/s.

For the thrust force measurement, the turbine tower is mounted on

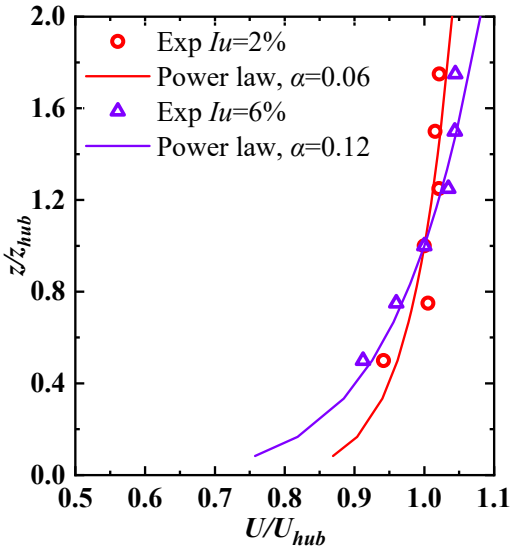

(a) Normalized mean wind velocity profile of upstream wind flow

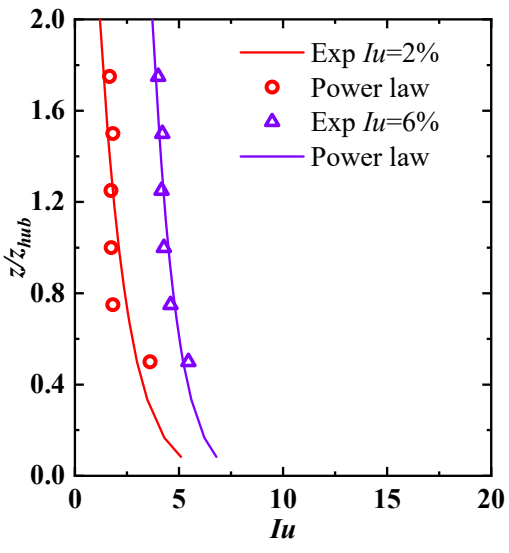

(b) Turbulence intensity profile of upstream wind flow

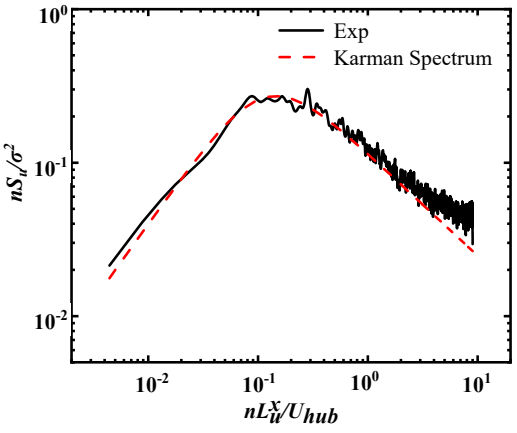

(c) Wind velocity spectrum at hub height for case of $I_{u,hub}$ = 6%

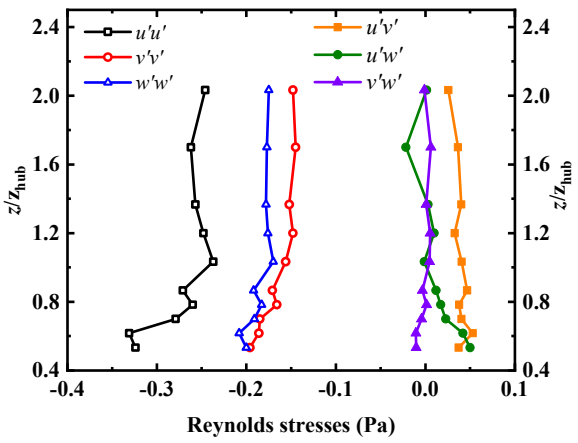

(d) Reynolds stresses of $I_{u,hub}$ = 6%

Fig. 8. Characteristics of incoming flow in wind tunnel test.

an ATI Delta six-axis high-frequency force balance. The calibrated ranges of ATI force balance are ±165 N in the streamwise, lateral and vertical directions with measurement uncertainty lower than 1%.

The thrust force T_{rb} under the rotating state of the wind turbine model and that of the tower and nacelle (without blades) T_{rn} are measured respectively. Since the high-speed operation of the wind turbine model driven by the motor could generate the thrust forces on itself, the thrust T_{nb} of the wind turbine under the rotating state in the absence of incoming wind speed is also measured. Then the net thrust T of wind blades under the design wind speed is determined by $T = T_{rb} - T_{rn} - T_{nb}$. Note that the subtraction of T_{nb} is due to the approximate linear relationship between T_{rb} and T_{nb}, which is shown in Fig. 9.

For the wake measurement in the wind tunnel test, the constant temperature hot-wire anemometry (CTA) is used to measure the wind speed and turbulence intensity. The CTA probe is made of gold-plated tungsten wire with a diameter of 4.5 μm, and the frequency response is 50 Hz. Dantec data acquisition instrument is adopted for high-fidelity data sampling. As shown in Fig. 10, the CTA probe is placed at different streamwise locations downstream of the wind turbine model (y/D = 4, 6, 8, and 10) and a total of 42 measurement positions are set for each vertical plane. Both the sampling of wake velocity and force measurements are at the rate of 500 Hz and with a duration of 60 s to ensure the statistical convergence of experimental measurements.

5. Results of thrust forces and turbine wakes

Firstly, this section presents the thrust coefficients measured for both D151-5 MW and D120-2 MW wind turbine models. Secondly, the wakes of the turbine model with thrust-matched blades are also given in the context of the wake velocity deficit and turbulence intensity, which are further compared with the analytical wake model.

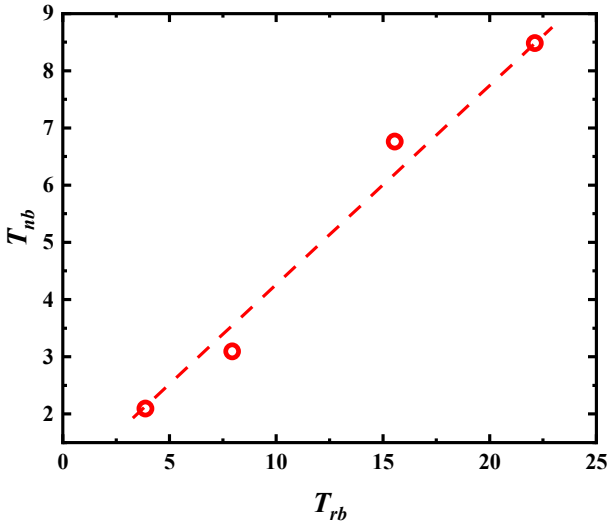

Fig. 9. Relationship between T_{rb} and T_{nb}.

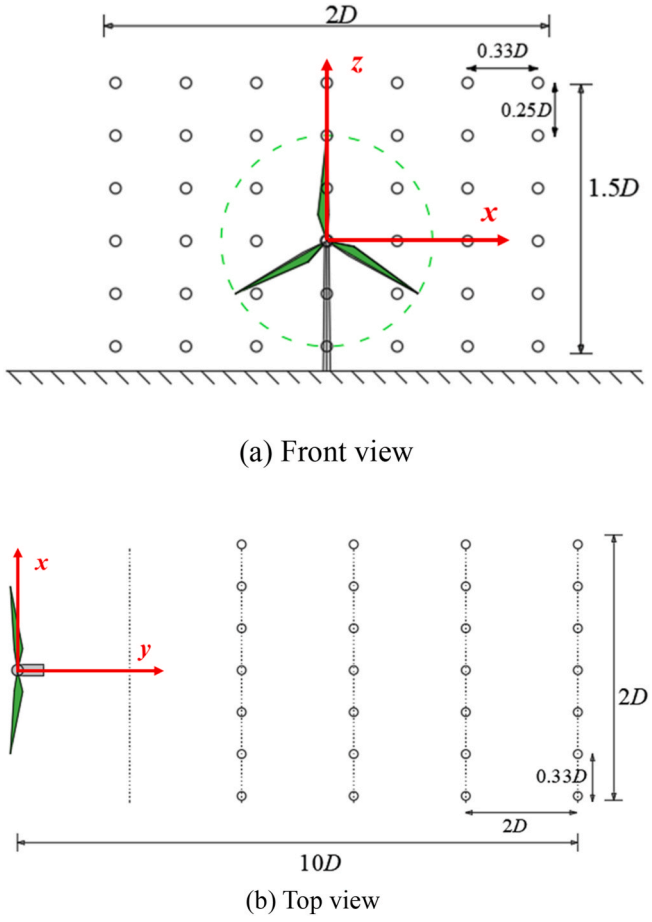

Fig. 10. Measurement locations in wind tunnel test.

5.1. Validation of thrust coefficients for reduced-scale wind turbine

Fig. 11 shows the experimental results of thrust coefficients for both D151-5 MW and D120-2 MW wind turbine models with geometrically-scaled and thrust-matched blades at different incoming wind speeds. As expected, the thrust coefficient of the geometrically-scaled blade model is significantly underestimated from the full-scale one. However, the thrust coefficients with redesigned, optimized blades could satisfactorily match the full-scale ones for both D151-5 MW and D120-2 MW wind turbines. This indicates that the proposed optimization methodology in this study is of great necessity for the thrust-match purpose and could well produce the small-scale blades satisfying the prescribed requirement of thrust similarity.

To elucidate the effects of pitch angle control on the thrust coefficients, the corresponding experimental results of the D151-5 MW turbine model with geometrically-scaled blades are included in Fig. 11 (b) under different pitch angles β in the range of $-30°\sim10°$. The incoming wind speed U_{hub} is 6 m/s and the rotor speed is 1942 rpm with a TSR of 10.3. As compared to C_T at $\beta = 0°$, the thrust coefficient at the pitch angle of $-20°$ is slightly augmented, but the counterpart at $\beta = 10°$declines. As a result, pitch angle control plays a more pronouncing role in lowering the thrust coefficient rather than increasing it. Therefore, it could hardly be used for the thrust-matched model tests.

5.2. Wake results of the wind turbine model with thrust-matched blades

In this section, the wake distributions of the wind turbine model under different upstream flow characteristics are measured and compared with the new Gaussian-based analytical wake model (NGW) by Ishihara and Qian (2018) for validation purposes.

Fig. 12 shows the comparisons of experimental and analytical profiles of wake velocity and turbulence intensity at the hub height located at different streamwise positions of $y/D = 4$, 6, 8, and 10. It can be seen that the wake measurements from the wind tunnel tests are generally consistent with those from NGW. This reveals that the wind tunnel tests of the small-scale wind turbine model by the proposed optimization methodology could rationally and reasonably reproduce the turbine wakes.

Profiles of the wake velocity and turbulence intensity under the scenarios of the same wind speed and different turbulence intensities are also compared in Fig. 12. The wake velocity characteristics under the low turbulence intensity wind condition of $I_u = 2\%$ are featured by larger velocity deficit, longer recovery length, but narrower wake width than those under high turbulence intensity with $I_u = 6\%$. And the wake turbulence intensity in the case of $I_u = 2\%$ is characterized by higher additional magnitude and longer recovery length, and wider wake width as compared with those in the case of $I_u = 6\%$.

Fig. 13 and Fig. 14 show the vertical plane contours of the wake with different turbulence intensities at the downwind distance y = 4*D*, where the dotted circle is the range of the wind turbine rotor. Likely, the spatial distributions of both wake velocity deficit and turbulence intensity are consistent with those revealed in Fig. 12. And the wake center, defined as the point where the velocity deficit is maximum at each vertical plane, is observed to vertically move downwards about 0.07*D*. In this study, the distance by which the wake center sinks is about 0.18*D* with the upstream turbulence intensity of 6%, while the counterpart is about 0.25*D* with the upstream turbulence intensity of 2%, which sinks more by 38.9%. Similar observations can be found in the experimental work done by Bastankhah and Porté-Agel (2016). The experimental results are horizontally symmetric but asymmetric in the vertical direction. This is attributed to the combined effects of nacelle and tower along with the upstream ABL flows (O'brien et al., 2018). A similar phenomenon is also revealed in the numerical simulations via the actuator line model (ALM) (Churchfield et al., 2015). In summary, the optimized blades considering the thrust force similarity are experimentally validated with high accuracy for far-wake characteristics in this study, meanwhile, it is still worth of investigating its validity in the near field wake measurements.

6. Conclusions

In this study, the optimization methodology for the thrust-matched scaled blades with a small scale-ratio is proposed and validated against the experimental measurements in the wind tunnel. The main

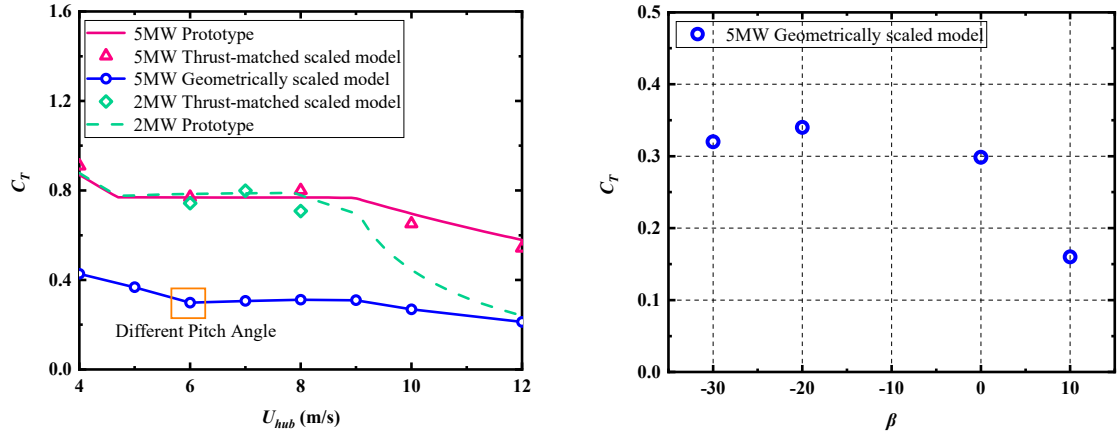

(a) Thrust coefficient of D151 and D120 at different wind speeds

(b) Thrust coefficient of D151 under different pitch angles (U_{hub}=6m/s)

Fig. 11. Thrust coefficient of D151 and D120 blades.

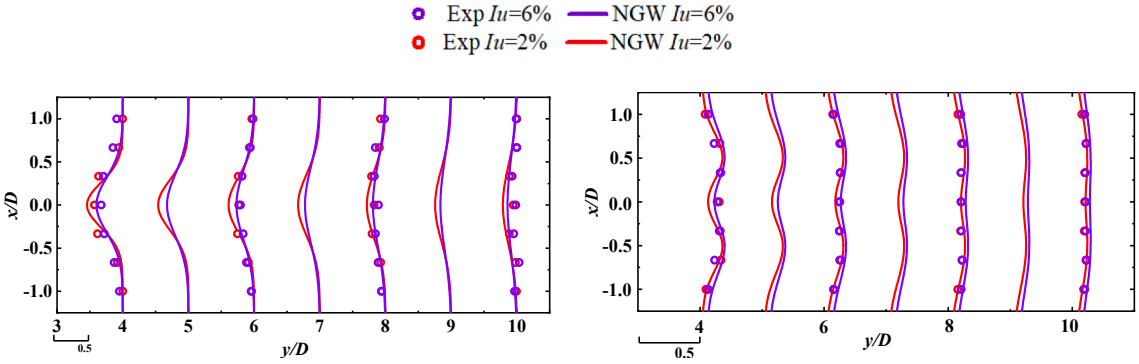

(a) Velocity distributions

(b) Turbulence intensity distributions

Fig. 12. Wake distributions for the thrust-matched model under U_{hub} = 10.4 m/s and Iu = 2%, 6%.

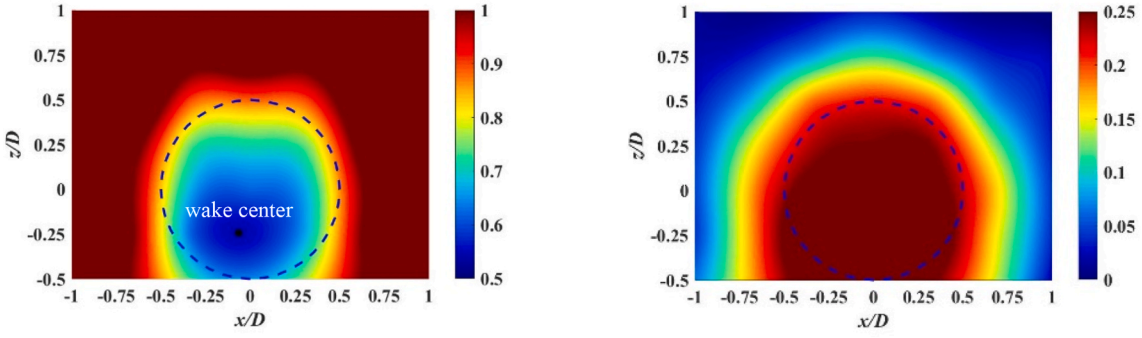

(a) Velocity distributions

(b) Turbulence intensity distributions

Fig. 13. Contours of wake distributions at y/D = 4 for the thrust-matched model under U_{hub} = 10.4 m/s and Iu = 2%.

conclusions and observations are summarized as follows:

(1) The wind turbine model with the redesigned blades by the proposed optimization methodology yields the thrust coefficient consistent with the prototype ones. Meanwhile, the thrust coefficient of the geometrically-scaled blade is only 30%–45% of the target one. And adjusting the pitch angle would exert prominent effects on reducing the thrust coefficient rather than increasing it. Therefore, it could hardly be used for the thrust-matched model tests.

(2) The comparison with the analytical wake model indicates that the wake characteristics obtained from the wind turbine model with thrust-matched blades are generally rational and valid in the context of wake velocity deficit and additional turbulence

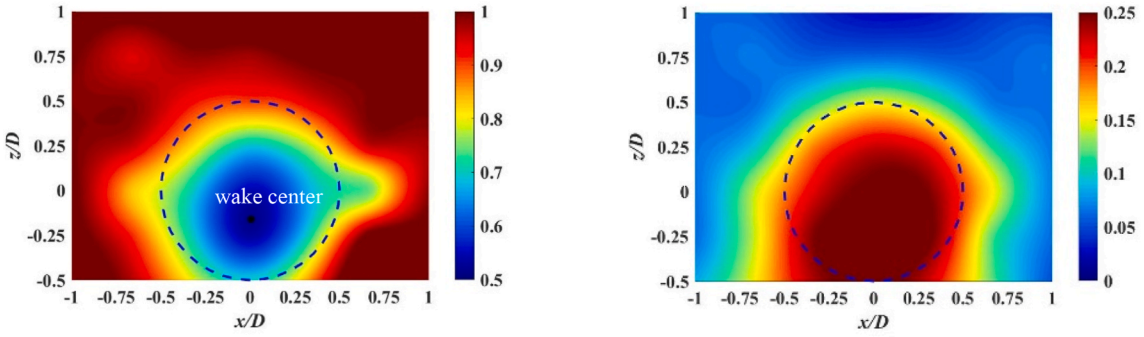

(a) Velocity distributions (b) Turbulence intensity distributions

Fig. 14. Contours of wake distributions at $y/D = 4$ for the thrust-matched model under $U_{hub} = 10.4$ m/s and $Iu = 6\%$.

intensity. Also, the effects of upstream turbulence intensity on the wind turbine wake evaluations could be well emulated. The vertically declining wake center is experimentally revealed, which becomes more apparent under lower upstream turbulence intensity.

CRediT authorship contribution statement

Guoqing Huang: Writing – review & editing, Supervision, Resources, Project administration, Funding acquisition. **Senqin Zhang:** Investigation, Formal analysis, Software, Validation, Visualization, Writing – original draft, Data curation. **Bowen Yan:** Conceptualization, Methodology, Formal analysis, Writing – review & editing, Supervision. **Qingshan Yang:** Formal analysis, Funding acquisition. **Xuhong Zhou:** Writing – review & editing. **Takeshi Ishihara:** Writing – review & editing.

Declaration of competing interest

The authors declare that they have no known competing financial interests or personal relationships that could have appeared to influence the work reported in this paper.

Data availability

Data will be made available on request.

Acknowledgments

The authors would like to acknowledge the financial support from the National Natural Science Foundation of China (Nos. 51878104 and 52178456), 111 Project of China (B18062), and Key Support Program of China for foreign experts (zcsf2021008).

References

Bastankhah, M., Porté-Agel, F., 2016. Experimental and theoretical study of wind turbine wakes in yawed conditions. J. Fluid Mech. 806, 506–541.
Chamorro, L.P., Porte-Agel, F., 2009. A wind-tunnel investigation of wind-turbine wakes: boundary layer turbulence effects. Boundary-Layer Meteorol. 132, 129–149.
Churchfield, M.J., Lee, S., Schmitz, S., Wang, Z., 2015. Modeling wind turbine tower and nacelle effects within an actuator line model. In: 33rd Wind Energy Symposium, Kissimmee, Florida.
Crespo, A., Hernandez, J., Frandsen, S., 1999. Survey of modelling methods for wind turbine wakes and wind farms. Wind Energy 2 (1), 1–24.
Dobrev, I., Maalouf, B., Troldborg, N., Massouh, F., 2008. Investigation of the wind turbine vortex structure. In: 14th International Symposium on Applications of Laser Techniques to Fluid Mechanics, Lisbon, Portugal.
Drela, M., 1989. XFOIL: an analysis and design system for low Reynolds number airfoils. In: Conference on Low Reynolds Number Airfoil Aerodynamics. University of Notre Dame.
Duan, F., Hu, Z., Liu, G., Wang, J., 2016. Experimental comparisons of dynamic properties of floating wind turbine systems based on two different rotor concepts. Appl. Ocean Res. 58, 266–280.
Fowler, M.J., Kimball, R.W., Thomas, D.A., Goupee, A.J., 2013. Design and testing of scale model wind turbines for use in wind/wave basin model tests of floating offshore wind turbines. In: 32nd International Conference on Ocean, Offshore and Arctic Engineering, Nantes, France.
Howland, M.F., Bossuyt, J., Martínez-Tossas, L.A., Meyers, J., Meneveau, C., 2016. Wake structure in actuator disk models of wind turbines in yaw under uniform inflow conditions. J. Renew. Sustain. Energy 8 (4), 043301.
Hui, H., Yang, Z., Sarkar, P., 2012. Dynamic wind loads and wake characteristics of a wind turbine model in an atmospheric boundary layer wind. Exp. Fluid 52 (5), 1277–1294.
Ishihara, T., Qian, G.W., 2018. A new Gaussian-based analytical wake model for wind turbines considering ambient turbulence intensities and thrust coefficient effects. J. Wind Eng. Ind. Aerod. 177, 275–292.
Ishihara, T., Yamaguchi, A., Fujino, Y., 2004. Development of a new wake model based on a wind tunnel experiment. In: Glob. Wind Power. http://windeng.t.u-tokyo.ac.jp/ishihara/e/.
Iungo, G.V., 2016. Experimental characterization of wind turbine wakes: wind tunnel tests and wind LiDAR measurements. J. Wind Eng. Ind. Aerod. 149, 35–39.
Jensen, N.O., 1983. A Note on Wind Generator Interaction. Risφ National Laboratory for Sustainable Energy, Technical University of Denmark.
Jonkman, J.M., Marshall, L., Buhl, J., 2005. FAST User's Guide. National Renewable Energy Lab.
Lanzilao, L., Meyers, J., 2022. A new wake-merging method for wind-farm power prediction in presence of heterogeneous background velocity fields. Wind Energy 25, 237–259.
Li, C., Zhou, S., Shan, B., Hu, G., Song, X., Liu, Y., Hu, Y., Yiqing, X., 2021. Dynamics of a Y-shaped semi-submersible floating wind turbine: a comparison of concrete and steel support structures. Ships Offshore Struct. 1–21. https://doi.org/10.1080/17445302.2021.1937801, 0.
Lyu, P., Chen, W.L., Li, H., Shen, L., 2019. A numerical study on the development of self-similarity in a wind turbine wake using an improved pseudo-spectral large-eddy simulation solver. Energies 12 (4), 643.
Martin, H.R., 2011. Development of a Scale Model Wind Turbine for Testing of Offshore Floating Wind Turbine Systems. M.S. thesis, University of Maine.
Martin, H.R., Kimball, R.W., Viselli, A.M., Goupee, A.J., 2014. Methodology for wind/wave basin testing of floating offshore wind turbines. J. Offshore Mech. Arctic Eng. 136 (2).
Medici, D., Alfredsson, P.H., 2006. Measurements on a wind turbine wake: 3D Effects and bluff body vortex shedding. Wind Energy 9, 219–236.
O'brien, J.M., Young, T.M., Early, J.M., Griffin, P.C., 2018. An assessment of commercial CFD turbulence models for near wake HAWT modelling. J. Wind Eng. Ind. Aerod. 176, 32–53.
Shamsoddin, S., Porté-Agel, F., 2020. Effect of aspect ratio on vertical-axis wind turbine wakes. J. Fluid Mech. 889.
Shi, X., Sun, J., Zhong, S., Huang, D., 2021. Flow control of a stalled S809 airfoil using an oscillating micro-cylinder at different angles of attack. Renew. Energy 175, 405–414.
Tian, W., Ozbay, A., Hu, H., 2018. An experimental investigation on the aeromechanics and wake interferences of wind turbines sited over complex terrain. J. Wind Eng. Ind. Aerod. 172, 379–394.
Viterna, L., Janetzke, D., 1982. Theoretical and experimental power from large horizontal-axis wind turbines. In: NASA TM-82944. National Aeronautics and Space Administration. Lewis Research Center, Cleveland, OH.
Xie, S., Archer, C., 2015. Self-similarity and turbulence characteristics of wind turbine wakes via large-eddy simulation. Wind Energy 18, 1815–1838.
Xiong, X.L., Lyu, P., Chen, W.L., Li, H., 2020. Self-similarity in the wake of a semi-submersible offshore wind turbine considering the interaction with the wake of supporting platform. Renew. Energy 156, 328–341.
Yang, Z., Sarkar, P., Hu, H., 2011. An experimental investigation on the wake characteristics of a wind turbine in an atmospheric boundary layer wind. In: 29th AIAA Applied Aerodynamics Conference, vol. 3815, pp. 1–18 (June).